White Rose Research Online

eprints@whiterose.ac.uk
https://eprints.whiterose.ac.uk
Universities of Leeds, Sheffield and York

Deposited via The University of Leeds.

White Rose Research Online URL for this paper:
https://eprints.whiterose.ac.uk/id/eprint/184942/

Version: Accepted Version

Article:
Li, X, Stringer, LC and Dallimer, M (2022) The role of blue green infrastructure in the urban thermal environment across seasons and local climate zones in East Africa. Sustainable Cities and Society, 80. 103798. ISSN: 2210-6707

https://doi.org/10.1016/j.scs.2022.103798

© 2022, Elsevier. This manuscript version is made available under the CC-BY-NC-ND 4.0 license http://creativecommons.org/licenses/by-nc-nd/4.0/.

Reuse
This article is distributed under the terms of the Creative Commons Attribution-NonCommercial-NoDerivs (CC BY-NC-ND) licence. This licence only allows you to download this work and share it with others as long as you credit the authors, but you can't change the article in any way or use it commercially. More information and the full terms of the licence here: https://creativecommons.org/licenses/

Takedown
If you consider content in White Rose Research Online to be in breach of UK law, please notify us by emailing eprints@whiterose.ac.uk including the URL of the record and the reason for the withdrawal request.

UNIVERSITY OF LEEDS
University of Sheffield
UNIVERSITY of York

Title: The role of blue green infrastructure in the urban thermal environment across seasons and local climate zones in East Africa

Highlights

- Local climate zone (LCZ) classifications for East African cities were examined.
- Significant Land Surface Temperature (LST) differences occurred between LCZs.
- LST and Enhanced Vegetation Index (EVI) revealed seasonal variations across LCZs.
- Possible cooling effects of urban green blue infrastructure were identified.

Abstract

Rapid urbanisation and climate change are two major trends in Africa in need of further investigation. In this paper, the urban thermal environment and vegetation abundance in four East African cities (Khartoum, Addis Ababa, Kampala and Dar es Salaam) were characterised, providing new insights into the role and potentials of blue green infrastructure in differing climate regions. The Local Climate Zone (LCZ) framework was employed to detect the seasonal Land Surface Temperature (LST) and Enhanced Vegetation Index (EVI) derived from Landsat-8 data. Significant LST differences between LCZs in dry and rainy seasons were confirmed using a Welch's T test. The LCZs were found to offer potentially new approaches to investigating issues pertaining to urban heating in data-scarce regions. Greater surface urban heat island (SUHI) intensity during the rainy season was apparent in Khartoum and Addis Ababa, emphasising the importance of seasonality in urban thermal studies. Spatial

correlations between EVI and LST within each LCZ were analysed through Moran's I and further illustrated the complex relationships of vegetation and thermal behaviour in urban areas. Despite these complexities, urban blue green infrastructure was found to moderate the SUHI, with different types of intervention required across different LCZs.

Keywords

Surface urban heat island; Enhanced vegetation index; Blue green infrastructure; Climate change; Urbanisation; Thermal environment

1. Introduction

Urbanisation and climate change are two of the most important trends influencing global development (Rogers, 2012). The global population living in urban areas is expected to increase from today's 55% to 68% by 2050 (United Nations, 2019). The fastest rates of urbanisation will occur in the least developed regions of Asia and Africa (United Nations, 2019). Cities serve as engines of change, dominating economic progress, and offering the potential to pull more people out of poverty (Demuzere et al., 2021; Rogers, 2012). Meanwhile, challenges in natural resource management exacerbated by climate change in rural areas can act as a push factor, causing people to move into cities. Despite potential economic advantages of urban living, many who move to urban areas are at risk from various environmental and social challenges, particularly as the climate changes and more of the urban population is exposed to heat stress (He, Zhao, et al., 2021; Van De Walle et al., 2022).

Burgeoning urban populations require more land for housing and infrastructure (Boke-Olén et al., 2017; Omumbo et al., 2005), driving land use/ land cover transformation. Large amounts of natural surface are replaced by impervious surfaces, changing the patterns of biodiversity and ecosystem services in different ways across different climate zones and contexts. One of the most significant challenges is transformation-induced climate alteration; in particular, the urban heat island (UHI) effect. UHI refers to the temperature difference between an urban area and its surrounding rural area (Oke, 1982). UHI is caused by development and modification in urban infrastructure

(He, 2019), in areas where higher proportions of impervious surface store more heat and restrict natural radiative cooling potentials (Gunawardena et al., 2017; Kabano et al., 2021). UHI intensities are influenced by the local micro-climate, with important factors including urban morphology, biome, meteorological conditions, presence or absence of water bodies and vegetation cover (He, Wang, et al., 2021; Imhoff et al., 2010; Li et al., 2021). As the climate changes and urbanisation proceeds at pace, it is important to understand differences in these relationships across different cities and climate zones.

A lack of climatological observations and urban cover/use information has previously restricted the number and quality of systematic studies for African cities (Brousse et al., 2019; Brousse, Wouters, et al., 2020). This impediment has been gradually overcome by improved high-resolution remote-sensing data and enhanced modelling capacities (Brousse et al., 2019). Furthermore, observational approaches to investigating temperature heterogeneity between urban surfaces have improved through development of the concept of local climatic zones (LCZ). The LCZ framework provides a uniform and generally recognized classification of urban cover/use that allows the comparison of cities in terms of urban form and urban function (Geletič et al., 2019; Stewart et al., 2012). The LCZ framework classifies urban areas into 10 “built” and 7 “land cover” types, with a LCZ type defined as a region that is uniform in properties of surface cover, structure, material, and human activity. Each LCZ type characterises a particular surface thermal climate (Stewart and Oke, 2012). LCZs have

now been generated for cities globally (Bechtel et al., 2015; Ching et al., 2018), becoming a new standard for characterizing urban landscapes (Zhao et al., 2021), particularly following further simplification of the process of LCZ classification with the LCZ Generator (Demuzere et al., 2021). LCZs may offer the potential to better understand the role of blue and green areas within the landscape and their moderation of SUHI effects. Nevertheless, this has not yet been fully explored. This paper takes up this challenge and provides novel empirical insights that can guide planners on the use of blue green infrastructure (BGI) in different LCZs.

Although LCZ classification has been used in some African cities to study UHI (Ochola et al., 2020), vegetation growing season length (Kabano et al., 2021) and urban health issues (Brousse, Wouters, et al., 2020), existing studies tend not to focus on the urban thermal environment in Africa there. Nor do studies consider the role of blue green infrastructure (BGI) in shaping thermal outcomes in different LCZ, while few take a comparative approach encompassing multiple cities in different climate zones within Africa. Indeed, land surface temperature (LST) variations among LCZ types are less studied under different microclimatological conditions in Africa, compared to land cover types within a single city, which have gained a lot of attention in the UHI literature (Geletič et al., 2019).

The main aim of this study is to examine the suitability of the LCZ classification for urban thermal studies under varying microclimatological conditions in different

climate zones in Africa and to assess the role of BGI in explaining any thermal differences with a view to informing planning. By doing so, we advance knowledge into the role of BGI in the urban thermal environment within different LCZ. We address the following questions: (i) Does using LCZ classifications bring new understanding to quantifying UHI effects in African cities? (ii) How do LST and SUHI within LCZs change seasonally, and are seasonal variations similar between cities with different climates? (iii) What is the relationship between LST and EVI within LCZs in different seasons? (iv) What is the potential for the retention, restoration or construction of BGI to mitigate SUHI, and how does this potential vary in different cities and LCZ?

2. Method

2.1 Study areas

Four cities in East Africa across different climate zones (Köppen classification): Khartoum, Addis Ababa, Kampala, and Dar es Salaam, were selected in this study (Fig. 1). In general, these cities could be considered as the engines of their respective country's economy and social development, and thus their rapid urbanisation could be expected to result in increased UHI intensity. The largest city in 2021 in terms of permanent residents among the study cities is Dar es Salaam (6.21 million), followed by Khartoum (5.99 million), Addis Ababa (5.01 million), and Kampala (3.47 million). These cities are characterised by highly fragmented vegetation surrounded by dense residential, commercial, and industrial areas. Further, the cities vary in the type and length of seasonal variations in temperature and rainfall that they experience, allowing

us to explore seasonality in more depth (Borhara et al., 2020; USAID, 2020).

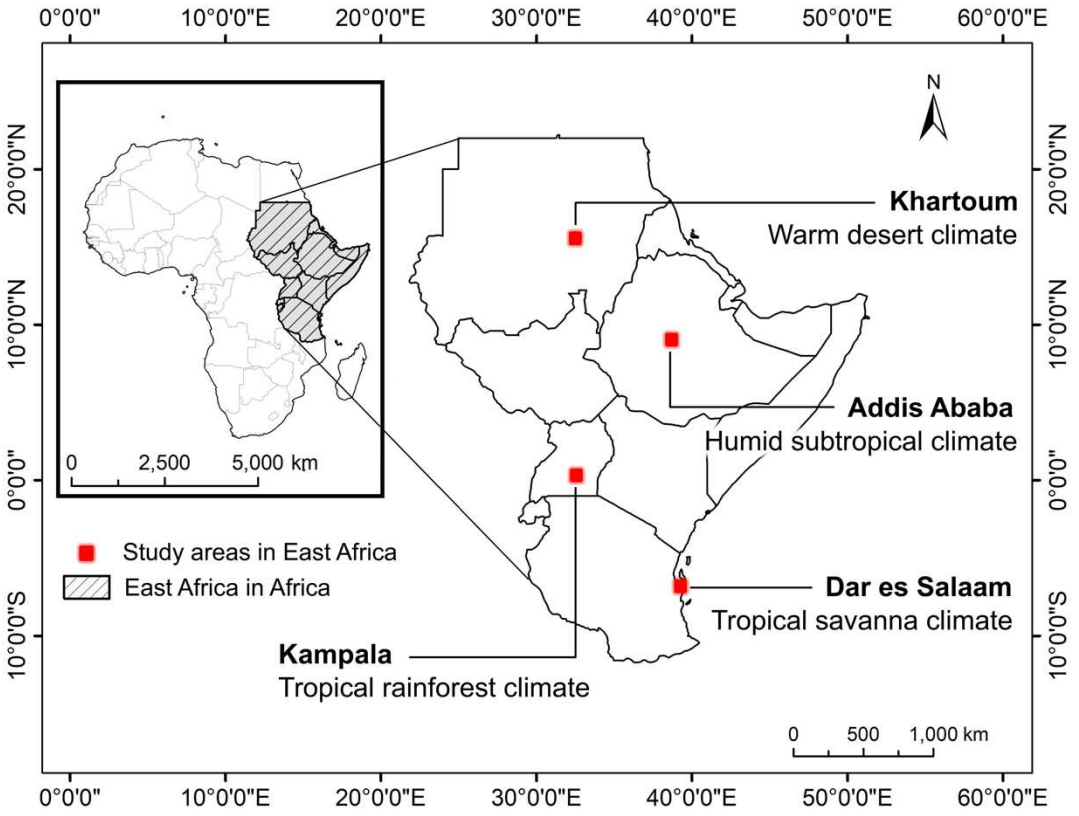

Fig. 1. Location of study cities in East Africa, with their climate zones (Köppen classification).

2.2 Data sources and analysis

2.2.1 LCZ classification

To reflect the spatial continuity of the urban built-up area outside the administrative boundaries (Lemoine-Rodríguez et al., 2020), we mapped the urban area boundary from Copernicus Global Land Cover Layers: CGLS-LC100 Collection 3 (Copernicus, 2021), downloaded via Google Earth Engine and processed in ARCGIS. Informal settlements, river channels and wetlands etc. were retained within the urban area

boundary.

Following the “Guidelines for Digitizing Training Areas” and the WUDAPT LCZ classification method (Bechtel et al., 2015; World Urban Database and Access Portal Tools, 2021), we digitised the training areas and mapped the LCZ for the study cities. Due to the cloud contamination across different times in different cities, the comparatively clear and distinct year of 2018 was selected as a representative year. Based on previous LCZ research in Africa (Bechtel et al., 2016; Brousse, Georganos, et al., 2020; Kabano et al., 2021; Ndetto et al., 2015), the most common LCZ classes were selected in each city. Depending on the area covered by each LCZ class and the feasibility of digitisation, the number of training samples per LCZ class ranged between 20 and 100. The overall process involved: (i) selecting and creating the training areas in Google Earth, (ii) submitting the training areas into the LCZ generator and getting results, (iii) using the results to revise the training areas, resubmitting and improving the accuracy to 70% or above in the final output.

2.2.2 LST/SUHI processing and relationship within LCZs

Rainy and dry seasons were defined based on previous research in East Africa (see supplementary document 1, Table 1). When mapping LST across different regions, finding clear images especially for the rainy season can be challenging. Cloud cover can mean that many Landsat tiles are required. To select the optimal images, we masked

out cloud and shadows from the images using pixel_qa band to get the 3-year periods' seasonal image collection for each city considering the years 2017, 2018 and 2019. We used the ee.Reducer and ee.ImageCollection.median of Google Earth Engine (GEE) to produce a cloud-free composite image from image collection (Google Earth Engine, 2022), for each season for each study city. Temporal aggregation and time series composition are two composition methods that have been widely used in multi-temporal Landsat images to reduce contamination by cloud and other problems (Phan et al., 2020). Time series composition involved a composition of cloud free images in a time series, while the temporal aggregation method used the metrics (e.g., median, mean and min/max) derived from time series images. Pre-processing in traditional time series composition methods requires significant storage capacity and access to high power computing (Phan et al., 2020). Recent advances in the temporal aggregation method significantly reduces data volume and generates data of equally high accuracy (Flood, 2013; Frantz et al., 2017; Phan et al., 2020). Nevertheless, despite being widely used in recent research (Chen et al., 2021; Richards et al., 2020), one major disadvantage of this method is that composite images from multi-year data produce land cover maps with lower accuracy than those from a single year, due to land cover change and loss of phenological consistency (Frantz et al., 2017). While a common strategy for generating an annual cloud free composite is to use images acquired over three years (Hu et al., 2019; Nyland et al., 2018; Xie et al., 2019), this research tried to capture the temporal variability on a seasonal time scale, so this challenge was avoided but phenological consistency was retained. Three years (2017,

2018, 2019) of satellite imagery over the dry and rainy seasons were composited to produce composite images representing the desired period (Flood, 2013).

Based on the USGS formulas (USGS, 2021b), the LST for the study areas was derived using the Mono-Window Algorithm (MWA) from Landsat data following five steps (Qin et al., 2001): (i) using the TIR band 10 to estimate brightness temperature; (ii) calculation of the Normalized Difference Vegetation Index (NDVI); (iii) obtaining proportional vegetation from NDVI values; (iv) calculation of land surface emissivity; and (v) calculation of the LST.

With the hypothesis that each LCZ class represents a distinct thermal characteristic (Stewart & Oke, 2012), we compared LCZ and LST. Firstly, the LSTs obtained from GEE and LCZ classes retrieved from the LCZ-generator were analysed in ArcGIS. As our data did not conform to the assumptions of ANOVA (Levene's test, p-value < 0.05) we ran Welch's t tests to detect the significance of the difference between LST and LCZ groups and then a post hoc Games-Howell test to determine which group caused the difference when the variances were not equal. The spatial distribution and variability of LSTs within LCZ classes were demonstrated in boxplots (See section 3.2, Fig. 4).

To investigate the seasonal variation of the SUHI in different LCZ classes, the SUHI intensity is defined as the difference between the LST value of a LCZ type when

compared with LCZ D (low plants) (Bechtel et al., 2019; Stewart & Oke, 2012). The formula for calculating SUHI intensity is as follows (Stewart & Oke, 2012):

$$SUHI_{LCZ_x} = LST_{LCZ_x} - LST_{LCZ_D} \quad (1)$$

Where LCZ_x represents a LCZ in study city, $SUHI_{LCZ_x}$ is SUHI intensity in LCZ_x, LST_{LCZ_x} is LST value in LCZ_x, and LST_{LCZ_D} is LST value in LCZ D.

2.2.3 EVI processing and correlation with LST within LCZs

We chose the Enhanced Vegetation Index (EVI) for characterising vegetation abundance as it retains sensitivity to the density of urban vegetation and also minimises canopy background variations (Kabano et al., 2021). EVI was calculated following USGS approaches (USGS, 2021a). The spatial variability influence of EVI on the performance of LST was analysed through spatial correlations between different study cities in the rainy and dry seasons. Through Geoda 1.20, the bivariate Moran's I function was used to represent the overall spatial correlation between seasonal LST and EVI within each LCZ class for the study cities (Anselin, 1996, 2020).

3. Results

3.1 LCZ classification

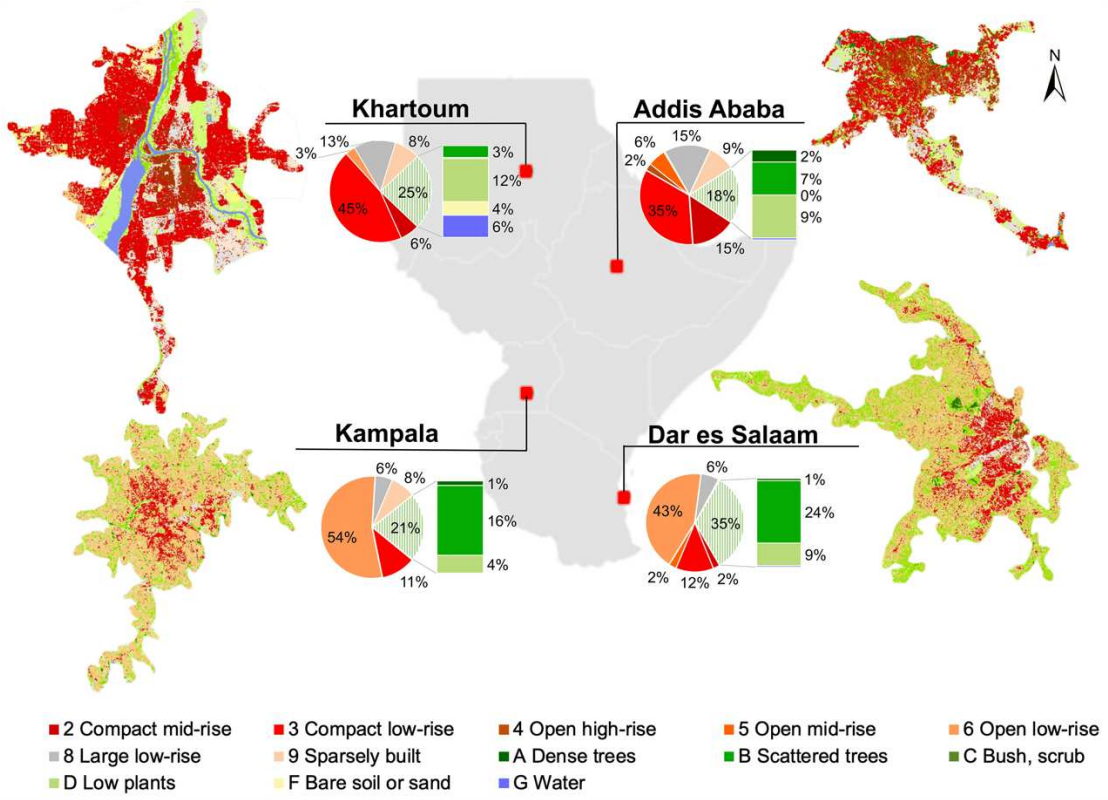

Fig. 2. LCZ maps for four study cities (Khartoum, Addis Ababa, Kampala, Dar es Salaam) within their urban cluster boundary. The original LCZ documents (training area information and accuracy) are provided in supplementary document 1, Table 2.

LCZ maps (Fig. 2) capture the morphological characteristics and the percentage of different LCZs across the four cities. Across all cities, the total areas of the built-up LCZs (LCZ 1-10) accounted for more than 50% of their area. Khartoum has the largest urban area among all the study cities. The urban area is dominated by compact commercial areas (LCZ 2) while residential areas (LCZ 3) have connected with adjacent cities, namely Khartoum North and Omdurman. These three cities have been integrated into a large urban cluster with no obvious boundary. The vegetation in southern Khartoum

is dominated by low plants (LCZ D) while the northern and north-western Khartoum megaregion are mainly bush and scrub (LCZ C).

The city centre and central business district in Addis Ababa are highly dense and compact so they are mainly classified as LCZ 2–4. There are also many isolated built-up areas in the southwestern part of Addis Ababa, which are mainly compact residential areas (LCZ 2) and factories (LCZ 8). This explains why the large low-rise LCZ account for 15.11% in Addis Ababa.

The LCZ map of Kampala indicates that residential areas with green infrastructure (LCZ 6) occupy most urban areas. A compact commercial centre (LCZ 2) and compact residential area (LCZ 3) are concentrated in the central downtown area. The rest of the areas are mostly classified as factories and sparsely built-up areas (LCZ 8 and LCZ 9). Scattered trees and farmland are interspersed in the urban areas. The total area of compact mid-rise and compact low-rise in Kampala accounted for only 0.13% and 10.90%. However, the open low-rise (LCZ 6) accounted for 54.18%.

A commercial centre (LCZ 2) and compact residential areas (LCZ3) are also found in Dar es Salaam. In addition, continuously connected factories are located in central and south-eastern areas. Scattered trees (LCZ B) accounted for 23.5% of the land area, an amount substantially greater than in Khartoum (3.05%), Addis Ababa (6.77%), and Kampala (16.23%).

3.2 LST and SUHI analysis

In Khartoum, LST varied between 23.9 °C and 40.3 °C in the rainy season, while in the dry season, LST varied between 26.5 °C and 38.6 °C. LST in Addis Ababa ranged from 13.1 °C to 33.0 °C in the rainy season, and from 17.4 °C to 35.5 °C in the dry season. For Kampala, LST varied from 19.4 °C to 30.9 °C in the rainy season, with this range expanding to 17.8 °C and 33.0 °C in the dry season. LST in Dar es Salaam was from 13.4 °C to 32.4 °C in the rainy season, and from 21.5 °C to 32.4 °C in the dry season.

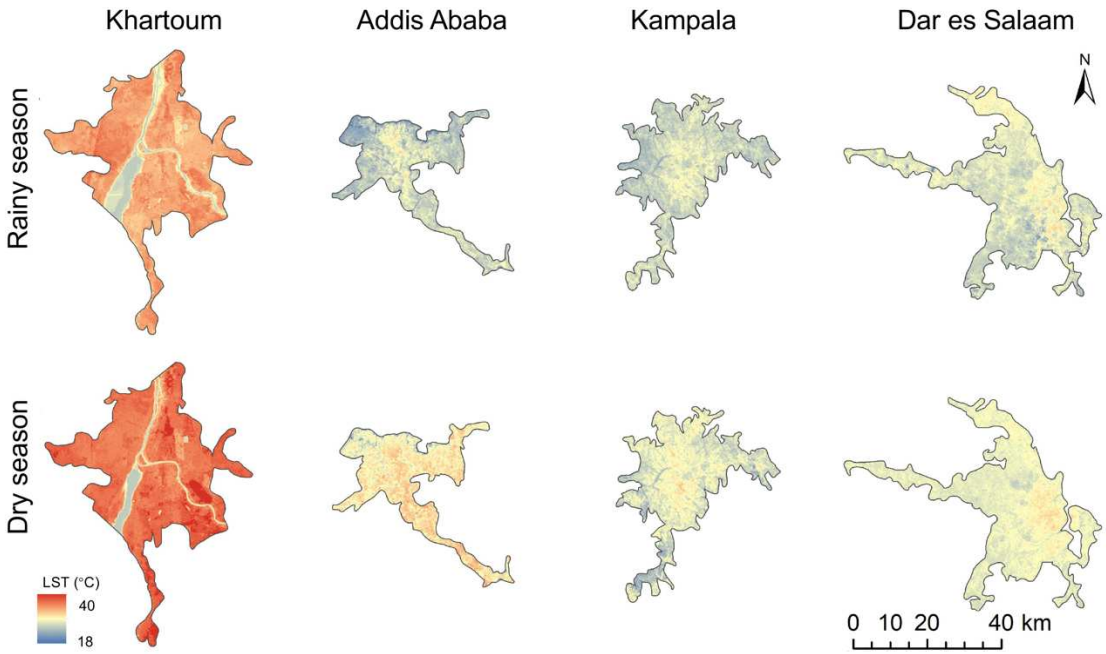

Fig. 3 The spatial distribution of LST in the rainy (top row) and dry (bottom row) seasons

For crosswise comparison among the LCZs, LST for all LCZ types in different season was

evaluated with the Welch's one-way ANOVA test (Fig. 4). In addition, each LCZ type in different seasons was compared by a paired sample test (Fig.4). The Welch's test results confirm the statistical significance of variances ($p < 0.00$) for all study cities in different seasons. The Games–Howell post hoc test was used for pairwise comparisons of mean LST value to identify their significant differences between LCZs (Fig. 5). Games-Howell test results indicate significant LST differences were observed in most LCZs during rainy and dry seasons.

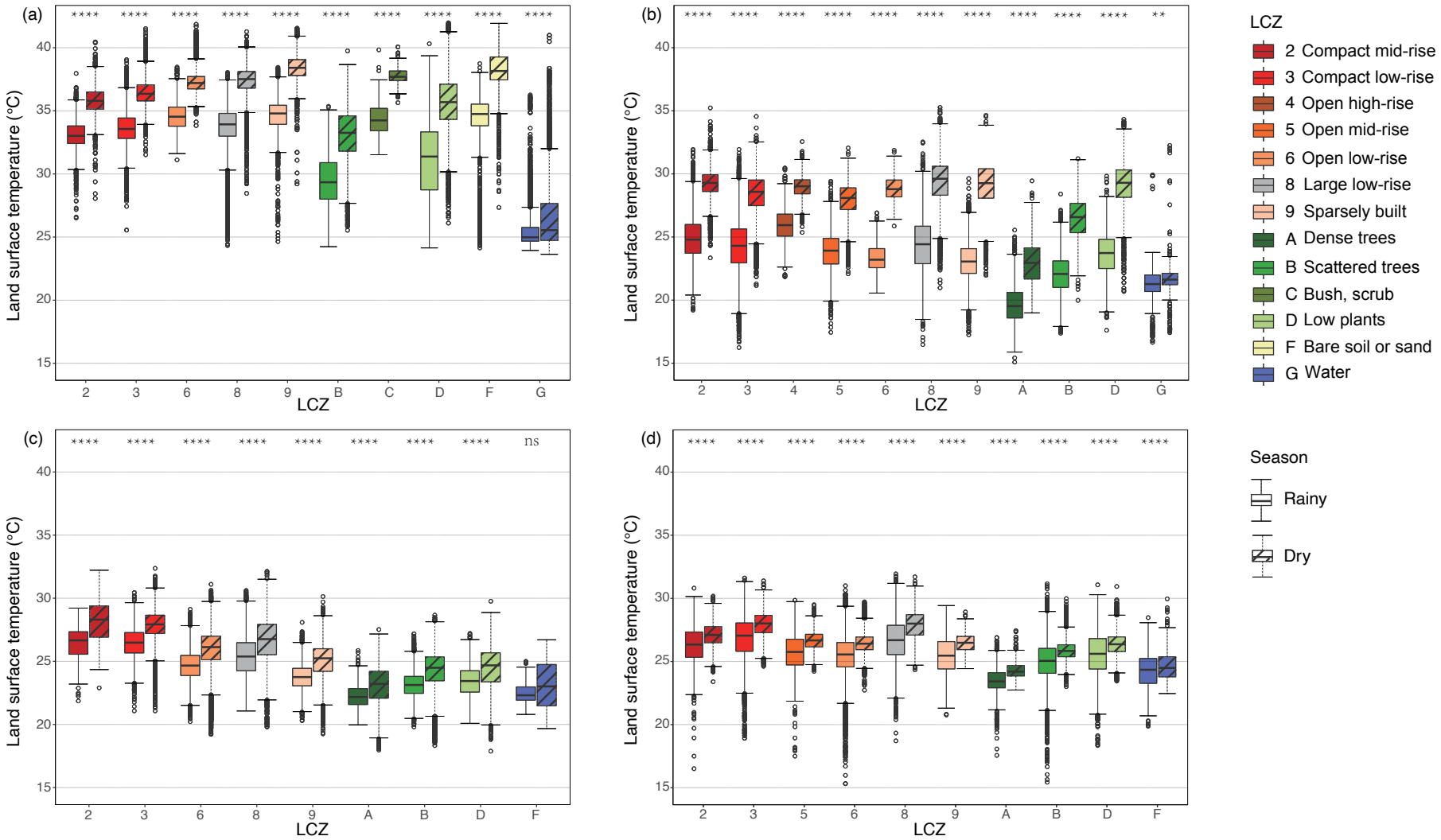

Fig. 4 Boxplots of the LST distribution in different LCZ in different cities (a) Khartoum, (b) Addis Ababa, (c) Kampala and (d) Dar es Salaam.

For the four cities considered in the research, the LSTs in the dry season are higher than in the rainy season, except for LCZ G (water) in Addis Ababa and Kampala. The LST of urban built-up LCZ classes (LCZ 2-9) was generally above that of the land cover classes (LCZ B-G) (Fig. 4). The differences in mean LST value across LCZ types varied greatly with the seasons. Even though there were relatively large variations in LST across different LCZ types, the general LST pattern was found to be similar during rainy and dry seasons. In particular, dense trees and water showed the coolest mean LST, and compact mid-rise buildings and large low-rise building presented more significant deviations from the mean LST for both seasons.

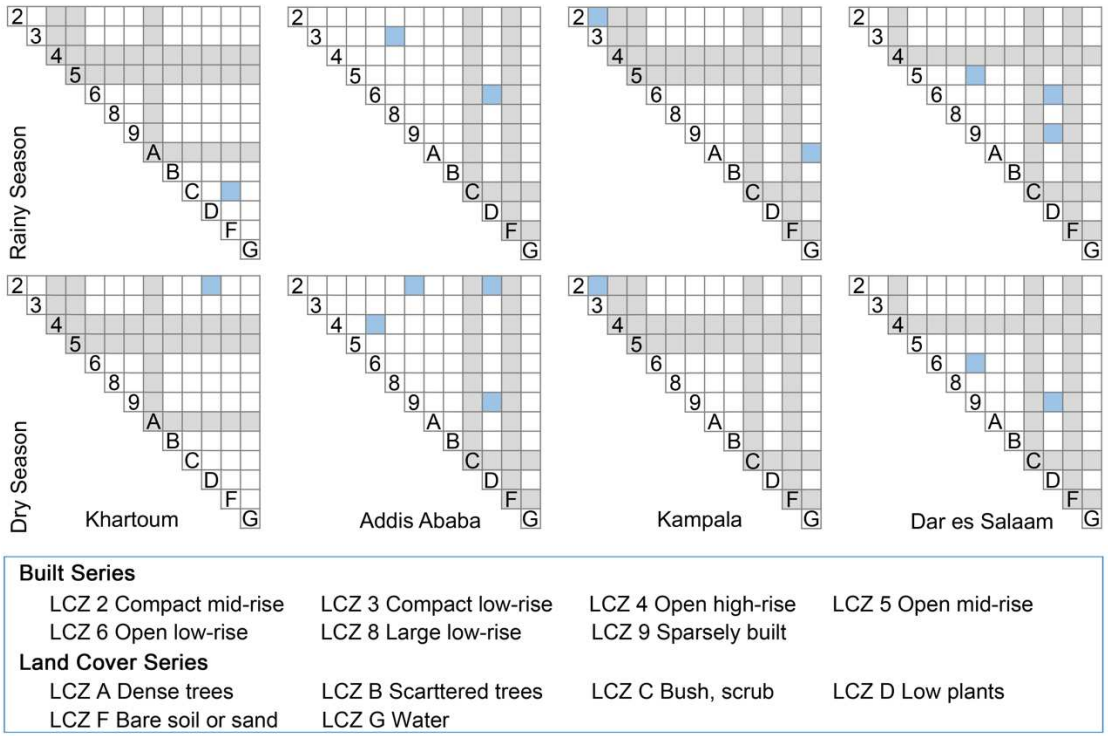

Fig. 5. The Games-Howell test results of differences in the LSTs between LCZ types. Grey squares represent non-representative LCZ classes, white squares stand for significantly different classes ($p < 0.05$), and blue squares represent LCZ pairs whose

are not significantly different ($p > 0.05$).

In Khartoum, there are large variations in SUHI across LCZ classes, and greater differences can be observed in the two seasons. In Khartoum, sparsely built areas (LCZ 9) during the rainy season have the highest SUHI (3.7 °C) among the built-up LCZ classes, followed by open low-rise built-up areas (LCZ 6) and large low-rise built areas (LCZ 8), with mean SUHI of 3.6 °C and 2.8 °C respectively. Scattered trees (LCZ B) and water (LCZ G) show the opposite trend in the two seasons with -1.6 °C and -5.6 °C mean SUHI. The pattern of SUHI in the dry season in Khartoum is similar to that of the rainy season: the highest SUHI was observed in LCZ 9 with 2.7 °C, with areas of scattered trees (LCZ B) and water (LCZ G) presenting stronger cooling by -2.7 °C and -9.2 °C.

Addis Ababa also has a higher SUHI intensity in the rainy season. During this season, compact mid-rise areas have the highest SUHI (2.3 °C), and second is the open high-rise areas, LCZ 2 (1.3 °C). SUHI in the dense tree zone (LCZ A) was -3.9 °C SUHI and in water areas (LCZ G) was -2.5 °C. While positive SUHI intensity was only detected in large low-rise (LCZ 8) 0.1 °C and compact mid-rise areas 0.02 °C in the dry season, water (LCZ G) presented -7.5 °C while areas with dense trees showed (LCZ A) -6.2 °C.

In Kampala, SUHI in all built type LCZs in both seasons are positive. Dry season SUHI is higher than in the rainy season, typically with 3.8 °C in LCZ 2 and 3.5 °C in LCZ 3 but

the SUHI in the rainy season is still strong, at 3.0 °C in LCZ 3 and 2.8 °C in LCZ 2. Dense trees play the most important role in urban cooling, supported by -1.4 °C SUHI in the dry season and -1.2 °C SUHI in the rainy season. Water also plays a critical cooling role with -1.4 °C in dry season and -0.9 °C in rainy season.

For Dar es Salaam, the LST in LCZs were statistically different between the two seasons, and SUHI was higher in the dry season. The city presented similar SUHI distribution patterns across different LCZs. The highest SUHI intensity was located in compact low rise (LCZ 3) areas with 1.6 °C in the dry season and 1.3 °C in the rainy season. Dense trees had a SUHI of -2.0 °C SUHI in the dry season and -2.1 °C in the rainy season. For water, SUHI was -1.7 °C in the dry season and -1.3 °C in the rainy season.

3.3 The relationship between LST and EVI

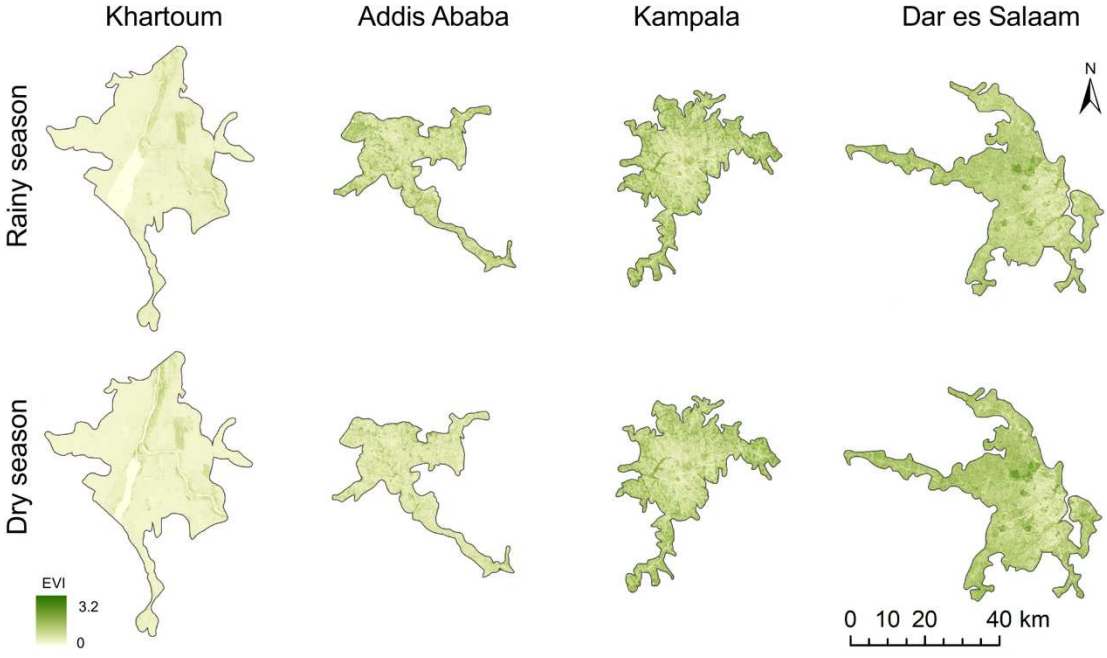

Fig. 6 The spatial distribution of EVI in the rainy (top row) and dry (bottom row) seasons

Fig. 6 shows the spatial distribution of EVI in the study cities. Differentiation of the vegetation cover across different macroclimate regions can be observed. The mean EVI value in Dar es Salaam (Tropical savanna climate) was similar to that of Kampala (Tropical rainforest climate), followed by Addis Ababa (Humid subtropical climate), and Khartoum (Warm desert climate). The mean EVI value is generally higher in the rainy season (1.04 in Kampala, 1.02 in Dar es Salaam, 0.81 in Addis Ababa, 0.21 in Khartoum), and decreases in the dry season (1.01 in Kampala, 0.57 in Addis Ababa, and 0.19 in Khartoum), except for an increase in Dar es Salaam which had a mean value of 1.13.

The bivariate Moran's I between LST and EVI was measured for the study cities. In Khartoum, Moran's I was 0.357 in the rainy season and 0.439 in the dry season, denoting a positive spatial relationship among the values of the adjacent variables. On the contrary, a relatively high negative spatial correlation was found in Kampala (−0. 54 in the rainy season and -0.43 in the dry season). Addis Ababa (−0. 18 in the rainy season and -0.06 in the dry season) and Dar es Salaam (−0.02 in the rainy season and -0.07 in the dry season) presented a weaker correlation.

To observe the internal relationship between the LST and EVI, we calculated the bivariate Moran's I between EVI and LST for each LCZ (Fig. 7). In general, LST in dense

trees (LCZ A) presents a negative correlation with EVI for all cities, while LST in scatted trees (LCZ B) and low plants (LCZ D) shows a variable correlation with EVI in the different cities and the different seasons. There were negative correlations between LST and EVI located in most LCZ types in Addis Ababa, Kampala and Dar es Salaam. In the dry season, highly negative correlations are found in Khartoum's LCZ 2; Addis Ababa's LCZ 3, LCZ D; Kampala's LCZ 2, LCZ 3 and LCZ 6. Highly positive correlations are found in Khartoum's LCZ B, LCZ D, LCZ F, LCZ G. As for the rainy season, highly negative correlations are found in Khartoum's LCZ 2 and LCZ D; Addis Ababa's LCZ 4; Kampala's LCZ 2, LCZ 3, LCZ 4 and LCZ A; Dar es Salaam's LCZ A. Highly positive correlations are found in Khartoum's LCZ 6, LCZ 9, LCZ F, LCZ G. The weakest correlation was observed in Dar es Salaam's LCZ 2 in the dry season with a value of -0.00. In Dar es Salaam, the bivariate Moran's I values fluctuate over a relatively small range: the magnitude of correlation is between -0.26 and 0.01, which shows less correlation compared to the other study cities.

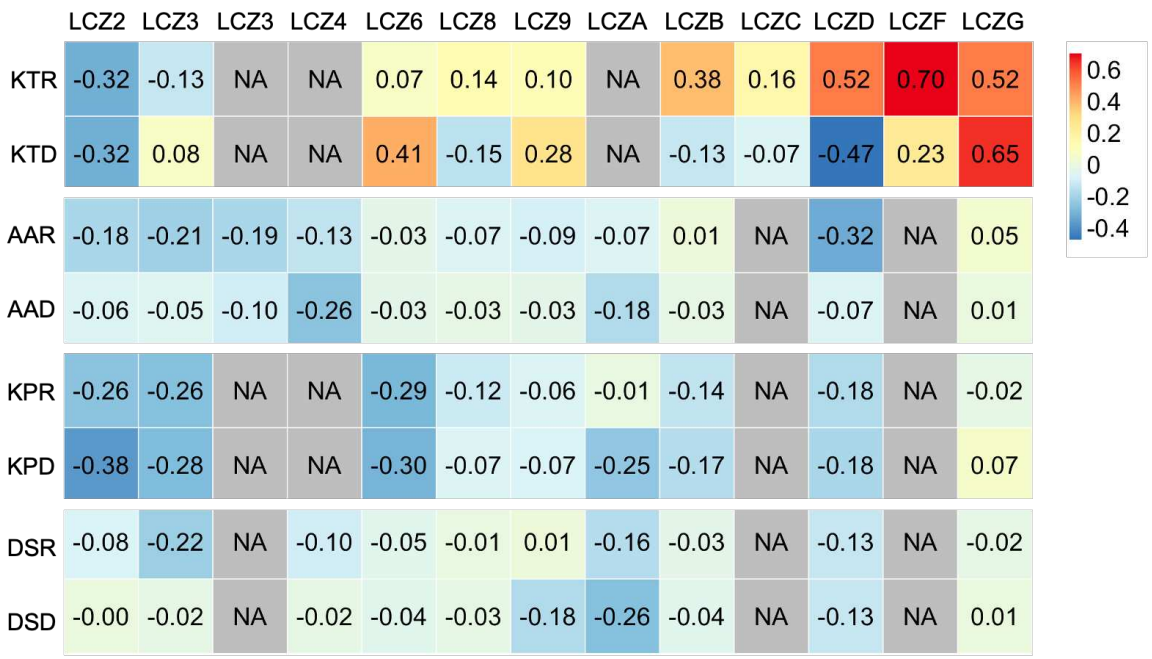

Fig. 7 Heatmap of global bivariate Moran's I between EVI and LST for each LCZ in different seasons. (NA indicates there is no specific LCZ class in corresponding city. The detailed Moran scatter plots are provided in supplementary document 2.

4. Discussion

4.1 LCZ classification for African urban issues

Local Climate Zones (LCZs) have been adopted as a standard way of analysing a wide variety of urban issues. While initial LCZ mapping procedures relied only on satellite data and software, which required time-consuming downloading and pre-processing, the cloud-based tool LCZ generator (Demuzere et al., 2021) addresses this shortcoming. The results of our analysis indicate that LCZ classification can be efficiently used across the different macroclimate regions and seasons in East Africa.

Significant LST differences between built and natural LCZs and within built types further support the suitability of LCZ for urban thermal environment analysis.

The LCZ maps illustrate clear variation in urban form across the study cities. Khartoum and Addis Ababa had a spatial structure that lies somewhere between fragmented and compact patterns, which is characteristic of cities undergoing rapid transformation (Lemoine-Rodríguez et al., 2020), dominated by diverse initial patterns and differential development trajectories (Lemoine-Rodríguez et al., 2020). Kampala and Dar es Salaam were characterized by a low-density and dispersed spatial pattern, which is closer to a fragmented urban form. This can be a consequence of sprawled urban development. Moderately fragmented urban forms can be beneficial in terms of a less intense UHI and higher accessibility to BGI (Schwarz et al., 2015). In contrast high urban fragmentation exacerbates impacts on the wider landscape and can increase urban pollution and exacerbate ecosystem services degeneration (Degefu et al., 2021; Huang et al., 2018; Tratalos et al., 2007). Africa is projected to experience rapid urban transformation in the coming decades (Oecd et al., 2020). Comparisons via spatiotemporal analysis of urban land densities have pointed out that urban forms in African cities are less compact than in China, Europe, and India (Xu et al., 2019). LCZ classification incorporates urban morphology into a mapping protocol, generating sufficient heterogeneity and design flexibility in the urban fabric (Perera et al., 2018; Stewart & Oke, 2012). Climate sensitive and data-scarce urban areas could harness such advantages, supporting the development of dynamic strategies for urban

development design and monitoring.

4.2 LST and SUHI differences in LCZ

Statistically significant LST differences in the study cities during different seasons further support the hypothesis that LCZs represent distinct surface temperatures (Stewart & Oke, 2012). The highest LST/SUHI intensities were generally located in LCZ 2, LCZ 3, LCZ 8, major commercial and industrial areas. The lowest LST/SUHI intensities were found in LCZ A and LCZ G, represented by dense trees and water. This corresponds with previous research findings in African cities (Brousse et al., 2019; Brousse, Wouters, et al., 2020; Kabano et al., 2021; Ochola et al., 2020). Generally, the temperature differences between cities can be expected to be related to the macro-climate, geographic region and urban area (Bechtel et al., 2019; Geletič et al., 2019; Potgieter et al., 2021). Even in different climate zones, there were statistically significant differences in mean LSTs between most LCZ. In this study, large low-rise (LCZ 8) LST in most cities was considerably higher than the other LCZ types. This may correspond to the large roof surfaces that frequently occur in LCZ 8. Surprisingly, LCZ 2 and LCZ 5 in Addis Ababa and Dar es Salaam, characterised by high-rise buildings, were the coolest built types, perhaps due to the shading effects of buildings. Similar distributions at certain time scales have also been observed in Toulouse, France (Kwok et al., 2019), Beijing, China (Zheng et al., 2019). The possible reasons for this can be summarised as follows: (i) The number of training areas for LCZ 2 and LCZ 5 affected the classification accuracy; (ii) Vegetation in LCZ 5 and shading effects from the high-

rise/mid-rise buildings provided cooler thermal environments (Kwok et al., 2019); (iii) The high proportion of vertical surfaces may affect the LST by preventing solar and surface interactions (Cilek et al., 2021; Zheng et al., 2019). This should nevertheless be further tested with more observations for high-rise buildings. Dense trees (LCZ A) and water (LCZ G) were identified as a lower LST zone, and the high LST variability of water would be expected, since temperature variation reflect the characteristics (depth, rate of flow, etc.) of individual water bodies (Geleti˘c et al., 2019). Considerable temperature differences between agriculture (LCZ D) and other zones were apparent. These might be due to the lower proportions of vegetation and the more robust radiation response of bare soil in different seasons (Geleti˘c et al., 2019).

4.3 LST/EVI correlation in different cities

Previous research has demonstrated that differences in LST depend on: i) variation in radiation intensity; ii) influences of evapotranspiration processes; iii) higher albedo of tree crowns during the vegetation period (Geletič et al., 2019; Gombe et al., 2017; Gunawardena et al., 2017; Stewart & Oke, 2012; Sun et al., 2019; Zhao et al., 2014). The present study demonstrated that LST/SUHI dynamics in different LCZs also vary between seasons. For example, both rainy and dry seasons EVI were negatively correlated with LST in LCZ 2, and LCZ 3 for Khartoum, Addis Ababa and Kampala, indicating a cooling potential of increasing green space cover percentage in these LCZ types. Positive correlations were found in LCZ 6, LCZ 8, LCZ 9 during Khartoum's rainy season, also a higher SUHI was detected in this period. For Dar es Salaam, the most

negative correlation between LST and EVI was observed in the rainy season in compact low-rise areas (LCZ 3), but in the dry season it was located in areas with dense trees areas (LCZ A) and low plants (LCZ D). The interactions between seasonal UHI and urban vegetation phenology could limit the provision of beneficial ecosystem services, such as urban agricultural productivity and the regulation of human thermal comfort (Kabano et al., 2021). For year-long effectiveness, greening strategies should account for seasonal effects (Chun et al., 2018). Such variability provides theoretical and practical information for urban planners on maximising the BGI efficiency in mitigating the UHI (Guo et al., 2019), as an integral part of sustainable urban planning and as an adaptation to higher temperatures under climate change.

4.4 Implications for urban development

African cities have been shown to be the most dynamic in terms of expansion and change in urban form (Lemoine-Rodríguez et al., 2020), offering many potential opportunities to ensure these cities develop more sustainably (Lemoine-Rodríguez et al., 2020; Xu et al., 2019). Climate change has been recognised as one of the most pervasive and challenging issues to the sustainable development of this region (Du Toit et al., 2018). To ameliorate the expected overheating problem under a changing climate in the East African cities, cooling strategies could take advantage of urban morphological information through LCZ classification. The effects of solar radiation shading in mid- and high-rise buildings may lower LST (Yang, Ren, et al., 2021);

controlling the wind movements through the streetscape, as wind breezes are affected by buildings (Yang et al., 2019); enhancing ventilation through linear parks and wind corridors (Ochola et al., 2020; Yang, Wang, et al., 2021). Meanwhile, greater attention could be paid to the potential applications of BGI to microclimate regulation. LCZs have been used to classify the urban areas and help to select target locations to develop BGI (Emmanuel et al., 2015; Wang et al., 2021). Findings from the present research indicate which types of BGI could maximise cooling effects across seasons.

The cooling island effect of water (LCZ G) was confirmed by our results and ranges from -9.2 °C to -0.9 °C. The precise magnitude of the cooling effect depends on surrounding environmental conditions such as microclimate, urban development, wind conditions, temperature and humidity. Water is a core feature of urban blue spaces. Hence, to enhance cooling performance of LCZ G, city planners and policy makers should take advantage of seasonal variations in blue space (Völker et al., 2013); the quantity and spatial distribution of water bodies (Yang et al., 2015); and how cooling effects are distributed with distance from, and flow rates within, rivers (Geletič et al., 2019; Wood et al., 2013). Considering increasing flood-drought risks in East African cities (Kalantari et al., 2018), urban water retention and flood regulation functions need to cope with the seasonal variation and climate changes. These factors should be accounted for in blue infrastructure design (Douglas, 2018; Kalantari et al., 2018).

The cooling effect of dense trees (LCZ A) has also been demonstrated in the results,

ranging from -6.2 °C to -1.4 °C, indicating the necessity to retain and add areas of dense tree cover in urban areas. However, when planning such programmes, prioritising indigenous species can help avoid the detrimental effects of homogenization of urban biodiversity (Lemoine-Rodríguez et al., 2020; Mckinney, 2006). In general, indigenous trees also consume less water and can enhance groundwater recharge relative to faster-growing exotic species (Kagawa et al., 2009; Singh et al., 2022). The greater water use of exotic species is enhanced in hotter, wetter climates (Cavaleri et al., 2010). In South Africa, Australian Acacia invasions have significantly reduced surface water runoff, impacting ecosystem services and water security (De Lange et al., 2010; Morris et al., 2020). Conserving dense tree cover for their cooling effects should therefore focus on promoting preservation and restoration of local indigenous species (Mckinney, 2006), while future research should aim to understand differences in cooling effects between exotic and indigenous trees.

Compact built-up areas (LCZ 2, LCZ 3) were characterised by densely built environments with little or no vegetation (Van De Walle et al., 2022), and comparatively high temperatures. To mitigate SUHI by planting more vegetated areas, urban planners could take advantage of improving the evapotranspiration-based cooling influence of green space through urban canopy-layer conditions (Emmanuel & Loconsole, 2015; Gunawardena et al., 2017). Street trees, green roofs and green walls could improve evapotranspiration and the shadowing effect of vegetation for compact LCZ types in Khartoum, Addis Ababa and Kampala. Cool roofs with lower albedo

material to prevent sunlight radiation caused by reflection could be considered in Dar es Salaam (Cilek & Cilek, 2021), as slight correlations between LST and EVI were observed in most built-up LCZs. Sparsely built areas (LCZ 9) with high SUHI and a low vegetation index were observed in all our study cities. Such underdeveloped lands within urban areas could be considered a valuable commodity for dynamic urban development.

The temperature-regulation capacity of BGI can potentially reduce heat stress in urban areas, but the choice and design of BGI type and distribution should be coordinated across different LCZs. The effects of BGI on temperature regulation have not however been quantified sufficiently, and so remain underrepresented in research and in recommendations for action and planning. For example, strategic planning for UHI mitigation and energy savings has faced the practical concern of the trade-off between energy and water use, as the cooling effect of some vegetation types, such as grassland in an arid city, is highly dependent on the water supply (Bencheikh et al., 2012; Wang et al., 2016). Moreover, inappropriately designed bluespaces come with the risk of exacerbating heat stress during oppressive conditions (Gunawardena et al., 2017) and present other potential risks under climate change linked to flooding and vector-borne diseases. Incorporating public health awareness and interventions into urban planning at the earliest stages could help ensure that BGI achieves its full potential for public health (Lõhmus et al., 2015).

Rapid urbanisation inevitably results in a loss of natural land covers, an increase in the amount of vertical surfaces that are present associated with a densification of existing built infrastructure; something that is apparent across many LCZ classes. If urban populations continue to grow as projected (United Nations, 2019), current scattered trees (LCZ B), low plants (LCZ D) and water (LCZ G) in urban areas will be gradually replaced by compact mid-rise (LCZ 2), compact low-rise (LCZ 3), open low-rise (LCZ 6), and dense trees (LCZ A) will be in danger of disappearing. It is notable that LCZ 2, 3 and 6 have higher temperatures than LCZ A (dense tree). Therefore, urban planners and policymakers should optimise both the spatial configuration and the cooling effects of BGI when working with limited land resources, taking into account seasonal differences.

5. Conclusion

Under the LCZ framework, this study conducted several statistical analyses for comparative study in four East African cities. It revealed the LST/SUHI dynamics and the complex relationship between LST and EVI in different LCZ across seasons. The results supported the assertion that the LCZ classification and LCZ-generator can be efficiently used in future urban thermal studies in a more spatially explicit way. Suggestions were also given as to how BGI could potentially facilitate the implementation of UHI mitigating strategies to support sustainable urban development, as urbanisation and climate change continue at pace within Africa's cities.

Funding:
This research was funded by UK government's Natural Environment Research Council (NERC), grant number NE/R002681/1.

Supplementary document 1

Table 1. General season classification in study cities (Borhara et al., 2020; USAID, 2020). 20170701

City	Rainy Season	Processed in this study	Dry Season	Processed in this study
Khartoum	July-September	01-07-2017 to 01-10-2017 01-07-2018 to 01-10-2018 01-07-2019 to 01-10-2019	September-July	01-10-2017 to 01-07-2018 01-10-2018 to 01-07-2019 01-10-2019 to 01-07-2020
Addis Ababa	June-September	01-06-2017 to 01-10-2017 01-06-2018 to 01-10-2018 01-06-2019 to 01-10-2019	November-January	01-11-2017 to 01-02-2018 01-11-2018 to 01-02-2019 01-11-2019 to 01-02-2020
Kampala	March-November	01-03-2017 to 01-12-2017 01-03-2018 to 01-12-2018 01-03-2019 to 01-12-2019	December-February	01-12-2017 to 01-03-2018 01-12-2018 to 01-03-2019 01-12-2019 to 01-03-2020
Dar es Salaam	December-January-February (peak) March- May	01-12-2017 to 01-03-2018 01-12-2018 to 01-03-2019 01-12-2019 to 01-03-2020	June-August	01-06-2017 to 01-08-2017 01-06-2018 to 01-08-2018 01-06-2019 to 01-08-2019

Table 2. LCZ classed selected in this study

City name	LCZ type

	Built series	Land cover series
Khartoum	LCZ 2, LCZ 3, LCZ 6, LCZ 8, LCZ 9	LCZ 12 (B), LCZ 13 (C), LCZ 14 (D), LCZ 16 (F), LCZ 17 (G)
Addis Ababa	LCZ 2, LCZ 3, LCZ 4, LCZ 5, LCZ 6, LCZ 8, LCZ 9	LCZ 11 (A), LCZ 12 (B), LCZ 14 (D), LCZ 17 (G)
Kampala	LCZ 2, LCZ 3, LCZ 6, LCZ 8, LCZ 9	LCZ 11 (A), LCZ 12 (B), LCZ 14 (D), LCZ 17 (G)
Kampala	LCZ 2, LCZ 3, LCZ 5, LCZ 6, LCZ 8, LCZ 9	LCZ 11 (A), LCZ 12 (B), LCZ 14 (D), LCZ 17 (G)

References

Anselin, L. (1996). *The Moran scatterplot as an ESDA tool to assess local instability in spatial* (Vol. 4).

Anselin, L. (2020). Multivariate Local Spatial Autocorrelation. Retrieved from https://geodacenter.github.io/workbook/6c_local_multi/lab6c.html

Bechtel, B., Alexander, P. J., Böhner, J., Ching, J., Conrad, O., Feddema, J., Mills, G., See, L., & Stewart, I. (2015). Mapping Local Climate Zones for a Worldwide Database of the Form and Function of Cities. *ISPRS International Journal of Geo-Information, 4*(1), 199-219. doi:https://doi.org/10.3390/ijgi4010199

Bechtel, B., Demuzere, M., Mills, G., Zhan, W., Sismanidis, P., Small, C., & Voogt, J. (2019). SUHI analysis using Local Climate Zones—A comparison of 50 cities. *Urban Climate, 28*, 100451. doi:https://doi.org/10.1016/j.uclim.2019.01.005

Bechtel, B., See, L., Mills, G., & Foley, M. (2016). Classification of Local Climate Zones Using SAR and Multispectral Data in an Arid Environment. *IEEE Journal of Selected Topics in Applied Earth Observations and Remote Sensing, 9*(7), 3097-3105. doi:https://doi.org/10.1109/JSTARS.2016.2531420

Bencheikh, H., & Rchid, A. (2012). The Effects of Green Spaces (Palme Trees) on the Microclimate in Arides Zones, Case Study: Ghardaia, Algeria. *Energy Procedia, 18*, 10-20. doi:https://doi.org/10.1016/j.egypro.2012.05.013

Boke-Olén, N., Abdi, A. M., Hall, O., & Lehsten, V. (2017). High-resolution African population projections from radiative forcing and socio-economic models, 2000 to 2100. *Scientific Data, 4*(1), 160130. doi:https://doi.org/10.1038/sdata.2016.130

Borhara, K., Pokharel, B., Bean, B., Deng, L., & Wang, S.-Y. S. (2020). On Tanzania's Precipitation Climatology, Variability, and Future Projection. *Climate, 8*(2), 34. doi:https://doi.org/10.3390/cli8020034

Brousse, O., Georganos, S., Demuzere, M., Dujardin, S., Lennert, M., Linard, C., Snow, R., Thiery, W., & Van Lipzig, N. P. (2020). Can we use local climate zones for predicting malaria prevalence across sub-Saharan African cities? *Environmental Research Letters, 15*(12), 124051. doi:https://doi.org/10.1088/1748-9326/abc996

Brousse, O., Georganos, S., Demuzere, M., Vanhuysse, S., Wouters, H., Wolff, E., Linard, C., Van Lipzig, N. P. M., & Dujardin, S. (2019). Using Local Climate Zones in Sub-Saharan Africa to tackle urban health issues. *Urban Climate, 27*, 227-242. doi:https://doi.org/10.1016/j.uclim.2018.12.004

Brousse, O., Wouters, H., Demuzere, M., Thiery, W., Van De Walle, J., & Van Lipzig, N. P. M. (2020). The local climate impact of an African city during clear-sky conditions—Implications of the recent urbanization in Kampala (Uganda). *International Journal of Climatology, 40*(10), 4586-4608. doi:https://doi.org/10.1002/joc.6477

Cavaleri, M. A., & Sack, L. (2010). Comparative water use of native and invasive plants at multiple scales: a global meta-analysis. *Ecology, 91*(9), 2705-2715. doi:https://doi.org/10.1890/09-0582.1

Chen, Q., Zhong, C., Jing, C., Li, Y., Cao, B., & Cheng, Q. (2021). Rapid Mapping and Annual Dynamic Evaluation of Quality of Urban Green Spaces on Google Earth Engine. *ISPRS International Journal of Geo-Information, 10*(10), 670. doi:https://doi.org/10.3390/ijgi10100670

Ching, J., Mills, G., Bechtel, B., See, L., Feddema, J., Wang, X., Ren, C., Brousse, O., Martilli, A., Neophytou, M., Mouzourides, P., Stewart, I., Hanna, A., Ng, E., Foley, M., Alexander, P., Aliaga, D., Niyogi, D., Shreevastava, A., Bhalachandran, P., Masson, V., Hidalgo, J., Fung, J., Andrade, M., Baklanov, A., Dai, W., Milcinski, G., Demuzere, M., Brunsell, N., Pesaresi, M., Miao, S., Mu, Q., Chen, F., & Theeuwes, N. (2018). WUDAPT: An Urban Weather, Climate, and Environmental Modeling Infrastructure for the Anthropocene. *Bulletin of the American Meteorological Society, 99*(9), 1907-1924. doi:https://doi.org/10.1175/BAMS-D-16-0236.1

Chun, B., & Guldmann, J.-M. (2018). Impact of greening on the urban heat island: Seasonal variations and mitigation strategies. *Computers, Environment and Urban Systems, 71*, 165-176. doi:https://doi.org/10.1016/j.compenvurbsys.2018.05.006

Cilek, M. U., & Cilek, A. (2021). Analyses of land surface temperature (LST) variability among local climate zones (LCZs) comparing Landsat-8 and ENVI-met model data. *Sustainable Cities and Society, 69*, 102877. doi:https://doi.org/10.1016/j.scs.2021.102877

Copernicus. (2021). Copernicus Global Land Cover Layers: CGLS-LC100 Collection 3. Retrieved from https://developers.google.com/earth-engine/datasets/catalog/COPERNICUS_Landcover_100m_Proba-V-C3_Global

De Lange, W. J., & Van Wilgen, B. W. (2010). An economic assessment of the contribution of biological control to the management of invasive alien plants and to the protection of ecosystem services in South Africa. *Biological Invasions, 12*(12), 4113-4124. doi:https://doi.org/10.1007/s10530-010-9811-y

Degefu, M. A., Argaw, M., Feyisa, G. L., & Degefa, S. (2021). Dynamics of urban landscape nexus spatial dependence of ecosystem services in rapid agglomerate cities of Ethiopia. *Science of The Total Environment, 798*, 149192. doi:https://doi.org/10.1016/j.scitotenv.2021.149192

Demuzere, M., Kittner, J., & Bechtel, B. (2021). LCZ Generator: A Web Application to Create Local Climate Zone Maps. *Frontiers in Environmental Science, 9*(112). doi:https://doi.org/10.3389/fenvs.2021.637455

Douglas, I. (2018). The challenge of urban poverty for the use of green infrastructure on floodplains and wetlands to reduce flood impacts in intertropical Africa. *Landscape and Urban Planning, 180*, 262-272. doi:https://doi.org/10.1016/j.landurbplan.2016.09.025

Du Toit, M. J., Cilliers, S. S., Dallimer, M., Goddard, M., Guenat, S., & Cornelius, S. F. (2018). Urban green infrastructure and ecosystem services in sub-Saharan Africa. *Landscape and Urban Planning, 180*, 249-261. doi:https://doi.org/10.1016/j.landurbplan.2018.06.001

Emmanuel, R., & Loconsole, A. (2015). Green infrastructure as an adaptation approach

to tackling urban overheating in the Glasgow Clyde Valley Region, UK. *Landscape and Urban Planning, 138*, 71-86. doi:https://doi.org/10.1016/j.landurbplan.2015.02.012

Flood, N. (2013). Seasonal Composite Landsat TM/ETM+ Images Using the Medoid (a Multi-Dimensional Median). *Remote Sensing, 5*(12), 6481-6500. doi:https://doi.org/10.3390/rs5126481

Frantz, D., Röder, A., Stellmes, M., & Hill, J. (2017). Phenology-adaptive pixel-based compositing using optical earth observation imagery. *Remote Sensing of Environment, 190*, 331-347. doi:https://doi.org/10.1016/j.rse.2017.01.002

Geletič, J., Lehnert, M., Savić, S., & Milošević, D. (2019). Inter-/intra-zonal seasonal variability of the surface urban heat island based on local climate zones in three central European cities. *Building and Environment, 156*, 21-32. doi:https://doi.org/10.1016/j.buildenv.2019.04.011

Gombe, K., Asanuma, I., & Park, J. (2017, 23-28 July 2017). *Characterization of urban heat island (UHI) changes from MODIS times series using principal component analysis (PCA): Case of Dar es Salaam City Tanzania.* Paper presented at the 2017 IEEE International Geoscience and Remote Sensing Symposium (IGARSS).

Google Earth Engine. (2022). ee.ImageCollection.median Retrieved from https://developers.google.com/earth-engine/apidocs/ee-imagecollection-median

Gunawardena, K. R., Wells, M. J., & Kershaw, T. (2017). Utilising green and bluespace to mitigate urban heat island intensity. *Science of The Total Environment, 584-585*, 1040-1055. doi:https://doi.org/10.1016/j.scitotenv.2017.01.158

Guo, G., Wu, Z., & Chen, Y. (2019). Complex mechanisms linking land surface temperature to greenspace spatial patterns: Evidence from four southeastern Chinese cities. *Science of The Total Environment, 674*, 77-87. doi:https://doi.org/10.1016/j.scitotenv.2019.03.402

He, B.-J. (2019). Towards the next generation of green building for urban heat island mitigation: Zero UHI impact building. *Sustainable Cities and Society, 50*, 101647. doi:https://doi.org/10.1016/j.scs.2019.101647

He, B.-J., Wang, J., Liu, H., & Ulpiani, G. (2021). Localized synergies between heat waves and urban heat islands: Implications on human thermal comfort and urban heat management. *Environmental Research, 193*, 110584. doi:https://doi.org/10.1016/j.envres.2020.110584

He, B.-J., Zhao, D., Xiong, K., Qi, J., Ulpiani, G., Pignatta, G., Prasad, D., & Jones, P. (2021). A framework for addressing urban heat challenges and associated adaptive behavior by the public and the issue of willingness to pay for heat resilient infrastructure in Chongqing, China. *Sustainable Cities and Society, 75*, 103361. doi:https://doi.org/10.1016/j.scs.2021.103361

Hu, Y., & Hu, Y. (2019). Land Cover Changes and Their Driving Mechanisms in Central Asia from 2001 to 2017 Supported by Google Earth Engine. *Remote Sensing, 11*(5), 554. doi:https://doi.org/10.3390/rs11050554

Huang, C., Yang, J., & Jiang, P. (2018). Assessing Impacts of Urban Form on Landscape Structure of Urban Green Spaces in China Using Landsat Images Based on

Google Earth Engine. *Remote Sensing, 10*(10), 1569. doi:https://doi.org/10.3390/rs10101569

Imhoff, M. L., Zhang, P., Wolfe, R. E., & Bounoua, L. (2010). Remote sensing of the urban heat island effect across biomes in the continental USA. *Remote Sensing of Environment, 114*(3), 504-513. doi:https://doi.org/10.1016/j.rse.2009.10.008

Kabano, P., Lindley, S., & Harris, A. (2021). Evidence of urban heat island impacts on the vegetation growing season length in a tropical city. *Landscape and Urban Planning, 206*, 103989. doi:https://doi.org/10.1016/j.landurbplan.2020.103989

Kagawa, A., Sack, L., Duarte, K. e., & James, S. (2009). Hawaiian native forest conserves water relative to timber plantation: Species and stand traits influence water use. *Ecological Applications, 19*(6), 1429-1443. doi:https://doi.org/10.1890/08-1704.1

Kalantari, Z., Ferreira, C. S. S., Keesstra, S., & Destouni, G. (2018). Nature-based solutions for flood-drought risk mitigation in vulnerable urbanizing parts of East-Africa. *Current Opinion in Environmental Science & Health, 5*, 73-78. doi:https://doi.org/10.1016/j.coesh.2018.06.003

Kwok, Y. T., Schoetter, R., Lau, K. K.-L., Hidalgo, J., Ren, C., Pigeon, G., & Masson, V. (2019). How well does the local climate zone scheme discern the thermal environment of Toulouse (France)? An analysis using numerical simulation data. *International Journal of Climatology, 39*(14), 5292-5315. doi:https://doi.org/10.1002/joc.6140

Lemoine-Rodríguez, R., Inostroza, L., & Zepp, H. (2020). The global homogenization of urban form. An assessment of 194 cities across time. *Landscape and Urban Planning, 204*, 103949. doi:https://doi.org/10.1016/j.landurbplan.2020.103949

Li, X., Stringer, L. C., & Dallimer, M. (2021). The Spatial and Temporal Characteristics of Urban Heat Island Intensity: Implications for East Africa's Urban Development. *Climate, 9*(4), 51. doi:https://doi.org/10.3390/cli9040051

Lõhmus, M., & Balbus, J. (2015). Making green infrastructure healthier infrastructure. *Infection Ecology & Epidemiology, 5*(1), 30082. doi:https://doi.org/10.3402/iee.v5.30082

Mckinney, M. L. (2006). Urbanization as a major cause of biotic homogenization. *Biological Conservation, 127*(3), 247-260. doi:https://doi.org/10.1016/j.biocon.2005.09.005

Morris, T. L., Barger, N. N., & Cramer, M. D. (2020). Ecophysiological traits of invasive alien Acacia cyclops compared to co-occuring native species in Strandveld vegetation of the Cape Floristic Region. *Austral Ecology, 45*(1), 48-59. doi:https://doi.org/10.1111/aec.12827

Ndetto, E. L., & Matzarakis, A. (2015). Urban atmospheric environment and human biometeorological studies in Dar es Salaam, Tanzania. *Air Quality, Atmosphere & Health, 8*(2), 175-191. doi:https://doi.org/10.1007/s11869-014-0261-z

Nyland, K. E., E. Gunn, G., I. Shiklomanov, N., N. Engstrom, R., & A. Streletskiy, D. (2018).

Land Cover Change in the Lower Yenisei River Using Dense Stacking of Landsat Imagery in Google Earth Engine. *Remote Sensing, 10*(8), 1226. doi:https://doi.org/10.3390/rs10081226

Ochola, E. M., Fakharizadehshirazi, E., Adimo, A. O., Mukundi, J. B., Wesonga, J. M., & Sodoudi, S. (2020). Inter-local climate zone differentiation of land surface temperatures for Management of Urban Heat in Nairobi City, Kenya. *Urban Climate, 31*, 100540. doi:https://doi.org/10.1016/j.uclim.2019.100540

Oecd, Sahel, & Club, W. A. (2020). *Africa's Urbanisation Dynamics 2020*.

Oke, T. R. (1982). The energetic basis of the urban heat island. *Quarterly Journal of the Royal Meteorological Society, 108*(455), 1-24.

Omumbo, J. A., Hay, S. I., Snow, R. W., Tatem, A. J., & Rogers, D. J. (2005). Modelling malaria risk in East Africa at high-spatial resolution. *Tropical Medicine & International Health, 10*(6), 557-566. doi:https://doi.org/10.1111/j.1365-3156.2005.01424.x

Perera, N. G. R., & Emmanuel, R. (2018). A “Local Climate Zone” based approach to urban planning in Colombo, Sri Lanka. *Urban Climate, 23*, 188-203. doi:https://doi.org/10.1016/j.uclim.2016.11.006

Phan, T. N., Kuch, V., & Lehnert, L. W. (2020). Land Cover Classification using Google Earth Engine and Random Forest Classifier—The Role of Image Composition. *Remote Sensing, 12*(15), 2411. doi:https://doi.org/10.3390/rs12152411

Potgieter, J., Nazarian, N., Lipson, M. J., Hart, M. A., Ulpiani, G., Morrison, W., & Benjamin, K. (2021). Combining High-Resolution Land Use Data With Crowdsourced Air Temperature to Investigate Intra-Urban Microclimate. *Frontiers in Environmental Science, 9*(385). doi:https://doi.org/10.3389/fenvs.2021.720323

Qin, Z., Karnieli, A., & Berliner, P. (2001). A mono-window algorithm for retrieving land surface temperature from Landsat TM data and its application to the Israel-Egypt border region. *International Journal of Remote Sensing, 22*(18), 3719-3746. doi:https://doi.org/10.1080/01431160010006971

Richards, D. R., & Belcher, R. N. (2020). Global Changes in Urban Vegetation Cover. *Remote Sensing, 12*(1), 23. doi:https://doi.org/10.3390/rs12010023

Rogers, W. (2012). Urbanization and the Global Climate Dilemma. Retrieved from https://www.newsecuritybeat.org/2012/07/urbanization-and-the-global-climate-dilemma-2/

Schwarz, N., & Manceur, A. M. (2015). Analyzing the Influence of Urban Forms on Surface Urban Heat Islands in Europe. *Journal of Urban Planning and Development, 141*(3), A4014003. doi:https://doi.org/10.1061/(ASCE)UP.1943-5444.0000263

Singh, K. K., Bhattarai, N., & Vukomanovic, J. (2022). Landscape-scale hydrologic response of plant invasion relative to native vegetation in urban forests. *Science of The Total Environment, 802*, 149903. doi:https://doi.org/10.1016/j.scitotenv.2021.149903

Stewart, I. D., & Oke, T. R. (2012). Local Climate Zones for Urban Temperature Studies. *Bulletin of the American Meteorological Society, 93*(12), 1879-1900.

doi:https://doi.org/10.1175/BAMS-D-11-00019.1
Sun, R., Lü, Y., Yang, X., & Chen, L. (2019). Understanding the variability of urban heat islands from local background climate and urbanization. *Journal of Cleaner Production, 208*, 743-752. doi:https://doi.org/10.1016/j.jclepro.2018.10.178
Tratalos, J., Fuller, R. A., Warren, P. H., Davies, R. G., & Gaston, K. J. (2007). Urban form, biodiversity potential and ecosystem services. *Landscape and Urban Planning, 83*(4), 308-317. doi:https://doi.org/10.1016/j.landurbplan.2007.05.003
United Nations. (2019). *World Urbanization Prospects 2018* Retrieved from New York: https://population.un.org/wup/Publications/Files/WUP2018-Highlights.pdf
USAID. (2020). *CLIMATE RISK PROFILE EAST AFRICA*. Retrieved from https://www.climatelinks.org/resources/climate-risk-profile-east-africa-regional
USGS. (2021a). Landsat Enhanced Vegetation Index. Retrieved from https://www.usgs.gov/core-science-systems/nli/landsat/landsat-enhanced-vegetation-index?qt-science_support_page_related_con=0#qt-science_support_page_related_con
USGS. (2021b). Using the USGS Landsat Level-1 Data Product. Retrieved from https://www.usgs.gov/core-science-systems/nli/landsat/using-usgs-landsat-level-1-data-product
Van De Walle, J., Brousse, O., Arnalsteen, L., Brimicombe, C., Byarugaba, D., Demuzere, M., Jjemba, E., Lwasa, S., Misiani, H., Nsangi, G., Soetewey, F., Sseviiri, H., Thiery, W., Vanhaeren, R., Zaitchik, B. F., & Van Lipzig, N. P. M. (2022). Lack of vegetation exacerbates exposure to dangerous heat in dense settlements in a tropical African city. *Environmental Research Letters, 17*(2), 024004. doi:https://doi.org/10.1088/1748-9326/ac47c3
Völker, S., Baumeister, H., Classen, T., Hornberg, C., & Kistemann, T. (2013). Evidence for the temperature-mitigating capacity of urban blue space—A health geographic perspective. *Erdkunde*, 355-371. doi:https://www.jstor.org/stable/23595377
Wang, Y., Ni, Z., Hu, M., Chen, S., & Xia, B. (2021). A practical approach of urban green infrastructure planning to mitigate urban overheating: A case study of Guangzhou. *Journal of Cleaner Production, 287*, 124995. doi:https://doi.org/10.1016/j.jclepro.2020.124995
Wang, Z.-H., Zhao, X., Yang, J., & Song, J. (2016). Cooling and energy saving potentials of shade trees and urban lawns in a desert city. *Applied Energy, 161*, 437-444. doi:https://doi.org/10.1016/j.apenergy.2015.10.047
Wood, C. R., Pauscher, L., Ward, H. C., Kotthaus, S., Barlow, J. F., Gouvea, M., Lane, S. E., & Grimmond, C. S. B. (2013). Wind observations above an urban river using a new lidar technique, scintillometry and anemometry. *Science of The Total Environment, 442*, 527-533. doi:https://doi.org/10.1016/j.scitotenv.2012.10.061
World Urban Database and Access Portal Tools. (2021). CREATE LCZ TRAINING AREAS. Retrieved from https://www.wudapt.org/digitize-training-areas/
Xie, S., Liu, L., Zhang, X., Yang, J., Chen, X., & Gao, Y. (2019). Automatic Land-Cover

Mapping using Landsat Time-Series Data based on Google Earth Engine. *Remote Sensing, 11*(24), 3023. doi:https://doi.org/10.3390/rs11243023

Xu, G., Dong, T., Cobbinah, P. B., Jiao, L., Sumari, N. S., Chai, B., & Liu, Y. (2019). Urban expansion and form changes across African cities with a global outlook: Spatiotemporal analysis of urban land densities. *Journal of Cleaner Production, 224*, 802-810. doi:https://doi.org/10.1016/j.jclepro.2019.03.276

Yang, B., Meng, F., Ke, X., & Ma, C. (2015). The Impact Analysis of Water Body Landscape Pattern on Urban Heat Island: A Case Study of Wuhan City. *Advances in Meteorology, 2015*, 416728. doi:https://doi.org/10.1155/2015/416728

Yang, J., Jin, S., Xiao, X., Jin, C., Xia, J., Li, X., & Wang, S. (2019). Local climate zone ventilation and urban land surface temperatures: Towards a performance-based and wind-sensitive planning proposal in megacities. *Sustainable Cities and Society, 47*, 101487. doi:https://doi.org/10.1016/j.scs.2019.101487

Yang, J., Ren, J., Sun, D., Xiao, X., Xia, J., Jin, C., & Li, X. (2021). Understanding land surface temperature impact factors based on local climate zones. *Sustainable Cities and Society, 69*, 102818. doi:https://doi.org/10.1016/j.scs.2021.102818

Yang, J., Wang, Y., Xue, B., Li, Y., Xiao, X., Xia, J., & He, B. (2021). Contribution of urban ventilation to the thermal environment and urban energy demand: Different climate background perspectives. *Science of The Total Environment, 795*, 148791. doi:https://doi.org/10.1016/j.scitotenv.2021.148791

Zhao, L., Lee, X., Smith, R. B., & Oleson, K. (2014). Strong contributions of local background climate to urban heat islands. *Nature, 511*(7508), 216-219. doi:https://doi.org/10.1038/nature13462

Zhao, Z., Sharifi, A., Dong, X., Shen, L., & He, B.-J. (2021). Spatial Variability and Temporal Heterogeneity of Surface Urban Heat Island Patterns and the Suitability of Local Climate Zones for Land Surface Temperature Characterization. *Remote Sensing, 13*(21), 4338. doi:https://doi.org/10.3390/rs13214338

Zheng, Z., Zhou, W., Yan, J., Qian, Y., Wang, J., & Li, W. (2019). The higher, the cooler? Effects of building height on land surface temperatures in residential areas of Beijing. *Physics and Chemistry of the Earth, Parts A/B/C, 110*, 149-156. doi:https://doi.org/10.1016/j.pce.2019.01.008